Spatially Controlled Functionalization and Chemical Manipulation to Fabricate Two-Dimensional Arrays of Gold Nanoparticles onto Indium Tin Oxide

Om P. Khatri[1,2*], Kuniaki Murase[1], and Hiroyuki Sugimura[1]

[1]Deptartment of Materials Science and Engineering, Kyoto University, Sakyo-ku, Kyoto 606-8501, Japan

[2]JSPS Fellow, Japan Society for the Promotion of Science, Tokyo, Japan

*E-mail address: khatriopk@gmail.com

ABSTRACT

We demonstrate the formation of two-dimensional (2D) arrays of gold nanoparticles (AuNPs) by controlled functionalization in a regular linear fashion, on the basis of the self-assembly and vacuum ultraviolet (VUV) lithography approaches. An octadecyltrimethoxysilane (ODS) monolayer, self-assembled on an indium tin oxide (ITO) surface, was exposed to VUV light (172 nm) through a photomask to construct the linear pattern by photodegradation of the ODS monolayer. Subsequently, an aminopropyltriethoxysilane (APS) monolayer was deposited on VUV-exposed sites by chemical vapor deposition. The immobilization of AuNPs on amino-terminated sites is due to the electrostatic attraction between citrate-stabilized AuNPs and amino groups of the APS monolayer, while the methyl-terminated sites remain unexposed. The structural organization of AuNPs in an alternating linear fashion was demonstrated by scanning electron microscope (SEM) analysis. The X-ray photoelectron microscopy (XPS) measurements were performed to probe the self-assembly of ODS, the APS monolayer, photopatterning and AuNPs immobilization.

KEYWORDS: indium tin oxide, monolayer, photolithography, gold nanoparticles, SEM, XPS.

1. Introduction

The immobilization of noble-metal nanoparticles onto the advanced electronic and optical materials are currently being investigated for their potential applications, such as to light-emitting diodes, organic optoelectronic devices, liquid crystal displays, surface plasmonic devices and chemical/biological sensors[1-4]. The physical properties of these nanoparticles are quite different from those of bulk, and these properties strongly depend on the particle size, shape, interparticle distance, particle composition and surface coating/functionalities on the nanoparticles[5-7]. The potential utilization of these nanoparticles for optoelectronic devices needs to develop the adaptable approaches for their assembly and/or integrate into desired structures and positions. Hence, considerable research efforts are now being directed towards the immobilization of gold nanoparticles into two- and three-dimensional (2D/3D) architectures[1,2,8-10].

The functionalization of indium tin oxide (ITO), which is a conductive optically transparent material, has been a subject of intense interest. There has been an increasing demand for microstructural fabrication on ITO surfaces with the assembly of nanoparticles onto the desired locations[9,11,12]. Microcontact printing (μCP)[8,13-15], dip-pen lithography[16], electron beam lithography[7,12], scanning probe lithography[9] and photolithography[17,18] have been demonstrated as fabricating tools in the last two decades. Electron beam lithography[7,12], dip pen lithography and scanning probe lithography[9] require very sophisticated equipment with high operation cost, which limits their exploitation at the application level. In microcontact printing, elastomer stamps have been used to immobilize the nano-objects at desired locations[13]. However, this method has a limited potential because of (a) the ease of contamination[19] during the transfer of physisorbed monolayer/nano-objects on the sample surface, (b) a higher defects level than that in photolithography and (c) the conformal contact between the stamp and sample surfaces with proper alignment[15]. Photolithography has been commonly employed for the micropatterning of the

organic monolayer with high throughput[18]. The resolution and quality of the photopattern can be monitored by many factors, such as the photomask, substrate properties, wavelength of UV light, and proximity gap between the sample surface and the light source. Wavelengths of the UV lights have the significant role to induce the photolysis of polymethylene chains either by photon-induced scission and the radical formation mechanism, which includes cross-linking and the creation of unsaturation[20], or by the photon-activated oxygen-induced photodegradation mechanism[21] for the patterning process. Here, we report microfabrication under VUV irradiation at 172 nm in wavelength, which is effectual and prompt in creating photopatterns on the surface by photochemical decomposition of the organic monolayer[18,21,22].

In this study, we developed binary monolayer systems with different terminal functionalities. First we formed the methyl-terminated (ODS) monolayer on an ITO surface; subsequently VUV patterning was performed to make the alternating linear features containing siloxane/silanol moieties, which show high affinity towards amino-terminated (APS) molecules. Alternating sites of methyl-terminated and amino-terminated monolayers are used to monitor the selective immobilization of AuNPs. Electrostatic affinity differences of AuNPs towards amino- and methyl-terminated monolayers make them effective for spatially controlled site immobilization of gold nanoparticles on ITO.

2. Experimental Procedure

A thin film (150 nm) of ITO deposited on soda lime glass was procured from Kuramoto Co. Ltd. Octadecyltrimethoxysilane (ODS; 95%) and aminopropyltriethoxysilane (APS; 97%) were purchased from Gelest and Aldrich, respectively, and were used as received. Gold nanoparticles (AuNPs; ϕ = 10.2 ± 1.7 nm) were procured from Sigma. Ultrapure water (UPW) was used throughout the sample preparation. Other reagents were of analytical grade.

ITO samples were thoroughly sonicated with ethanol and UPW. Subsequently, samples were immersed in a mixture of H_2O and H_2O_2 (5:2 v/v) for 40 minutes at over 100 °C, then washed with copious amounts of UPW and dried in a stream of dry nitrogen gas. Before ODS monolayer deposition, ITO samples were kept in the VUV/ozone treatment chamber for 20 min to burn off all carbonaceous contaminants. The very low water contact angle (0-2°), after the cleaning treatment confirmed the hydrophilicity on the ITO surface[23]. An ODS monolayer was formed by chemical vapor deposition[24]. Samples and a glass vessel, which contains 100 μL ODS, were placed together in a Teflon container under dry nitrogen atmosphere. The Teflon container was sealed with a cap and placed in an electric oven at 150 °C. After 3 h, the samples were removed from the oven and ultrasonically rinsed with ethanol for 10 min. Water contact angle on the ODS-modified ITO surface was found to be 105°±1, resulting in the formation of a methyl-terminated monolayer[22,24]. The ODS monolayer self-assembled on ITO was then irradiated with VUV light for 10 minutes through a photomask in contact with the sample surface. VUV patterning was performed under ambient conditions, where the presence of plenty of oxygen molecules facilitates the photodegradation of alkyl chains[21,25]. The photomask, employed in this study is a 2-mm thick quartz glass plate consisting of a 0.1-μm thick chromium pattern with a 10-μm wide linear window for VUV light. An APS monolayer was fabricated on the VUV-patterned template by chemical vapor deposition[24] at 100 °C using 10% (v/v) APS solution in toluene. After a 2-hour as deposition time, samples were sonicated successively in toluene, ethanol and UPW for 5 min each. APS molecules were assembled on VUV-exposed sites and masked regions remained untreated. In the final step, the binary monolayer-modified ITO samples were immersed in AuNPs aqueous solution for two hours, followed by rinsing with UPW.

X-ray photoelectron spectroscopy (XPS; Kratos Analytical, ESCA 3400) measurements were performed to monitor the elemental composition during each step of fabrication on the ITO surface, using Mg Kα radiation as the X-ray source. All

measurements were executed at 10 mA emission current and 10 kV acceleration voltage. The vacuum level during the measurements was kept in the range of 10^{-7} Pa. Since weak charging of the monolayer on ITO was recognized, the binding energies for all bands were aligned to the In $3d_{5/2}$ i.e., 445 eV. The atomic percentage on the sample surfaces was determined using the inbuilt XPS software "VISION2" considering the peak areas of the each band. It is based on the peak areas and their corresponding relative sensitivity factor (RSF), and provides the relative elemental composition, as shown in Table 1. The chemically distinct species for C 1s were resolved using a Gaussian-Lorentzian fitting program. The JEOL JSM-7400F field emission scanning electron microscope (FE-SEM) and Keyence VE-7800 scanning electron microscope (SEM) were used to examine the structural organization of AuNPs on the ITO surface and linear patterning features, respectively.

3. Results and Discussion

The ODS monolayer, formed by self-assembly approach on the ITO surface, works as a photoresist thin film. The ODS monolayer was exposed to VUV light at 172 nm wavelength for 10 minutes through a photomask, which generates linear pattern features by photodegradation of the ODS molecules on the VUV-exposed sites, as shown in Fig. 1. Atmospheric oxygen molecules play the vital role to induce the photopattern by absorbing VUV light (172 nm). Singlet oxygen atoms, which are formed by photon activation of oxygen molecules, have strong oxidative capability and oxidize the terminated methyl groups of the ODS monolayer to either –COOH or –CHO moieties[21]. The oxidation and subsequent degradation of alkyl chains progressed until complete photodegradation. VUV-exposed sites of the ODS monolayer became hydrophilic owing to the formation of the silanol and/or siloxane moieties, resulting in the creation of new vacancies for other surfactants, while the masked sites remained pristine. APS molecules, which have strong affinity towards silanol/siloxane, formed a spatially controlled monolayer on VUV-exposed sites, as illustrated in Fig. 1(c). The alternating arrangement of methyl- and amino-terminated

monolayers in the linear features facilitated the AuNPs immobilization on the modified ITO substrate with spatially controlled sites. The APS monolayer attracts the AuNPs because of electrostatic affinity between amino groups and citrate-stabilized gold[26].

Figure 2(a) shows the SEM image consisting of bright and dark linear features, which correspond to the AuNPs immobilized region (VUV exposed) and the methyl-terminated region (masked), respectively. Bright linear features were wider than the photomask window size (10 μm). We observed 13.2 ± 0.3 and 6.6 ± 0.3 μm widths of linear features consisting of AuNPs and masked regions, respectively. The broadening of the linear photoprinted features on the ODS-modified ITO surface was due to two possible reasons. The first reason may be the roughness of the ITO surface. Topographic images scanned by AFM over a 2 x 2 μm^2 area shows 2-3 nm peak-to-peak roughness. This roughness might be unable to make conformal contact between the photomask and the ODS-modified ITO surface, which allows the diffusion of some activated oxygen species to damage the ODS monolayer even in masked areas. These activated oxygen species are promptly deactivated when they collide with solid surfaces and are even able to partially degrade ODS molecules, particularly at the edge area of the masked regions. The partial degradation of ODS molecules was confirmed by appearance of CO and COO carbon peaks with significant intensity in the XPS measurements (Fig. 3). Another reason might be the reflection of some of the VUV photons from the ITO/glass interface. These reflected photons may go to the masked area and dissociate the ODS monolayer. To confirm this, we performed similar studies using silicon as a substrate, which is quite smooth compared to ITO, and did not observe the broadening of pattern features[27]. This study confirmed that VUV light reflections from the ITO/glass interface and the roughness of the ITO surface play significant roles in the damage of the masked ODS monolayer and the resultant broadening of pattern size.

A sub-monolayer of AuNPs on the amino-terminated sites is shown in Fig. 2(b) at high magnification. This image shows uniformly scattered organization of nanoparticles. AuNPs are negatively charged owing to the citrate coating, while the amino groups are positively charged in aqueous solution ($-NH_2 + H_2O \rightarrow -NH_3^+ + OH^-$). The immobilization of AuNPs onto the ITO surface originates from the electrostatic attractions between the negatively charged AuNPs and positively charged amino groups[26]. The repulsive interparticle interactions inhibit further immobilization of AuNPs onto the ITO surface before the close-packed state is reached. We observed the average surface density of AuNPs on the amino-terminated sites to be 1950 ± 50 AuNPs per μm^2.

XPS measurements were performed to achieve better understanding on the progress of surface modification in each step of fabrication. We mainly concentrated on C 1s, Si 2p, and Au 4f regions of the spectrum as these three elements are the characteristic components of ODS and APS monolayers, and AuNPs. The prime steps of the fabrication process were the backfilling of the VUV-exposed area by APS molecules, followed by the immobilization of AuNPs. Si 2p spectra measured in each step of the process are shown in Fig. 4(a). For the ODS monolayer, the Si 2p peak appeared at 102.9 eV. The increase of the Si 2p peak intensity after the backfilling of VUV-exposed sites confirmed the formation of the APS monolayer. C 1s spectra are shown in Fig. 4(b) for the same series of samples. For the ODS monolayer, a peak observed at 284.9 eV corresponds to the aliphatic carbon of ODS molecules. After VUV lithography on controlled sites through a photomask, a decrease in the peak intensity was noted, which was due to the photodegradation of carbon chains in the VUV-exposed area. During the subsequent backfilling with APS molecules, the C 1s peak intensity increased from 14% to 20% and a shift of 0.5 eV towards higher binding energy was noted. The detailed examination of the C 1s region in the XPS spectra during each step revealed clear differences in the chemical states of carbon. Figure 3(a) shows that the C 1s peak of the VUV-patterned ODS monolayer is a

combination of three different types of carbon. These were C-H/C-C, CO, and COO at 284.9, 286.2, and 288.5 eV, respectively[28]. The photochemistry involved in VUV lithography monitors the ratio of different types of carbon, which we have described separatly[27]. Backfilling of the VUV-exposed area was also confirmed by the increase in the C 1s peak intensity and the appearance of a new carbon peak at 285.8 eV attributed to C-NH_2 bonds and resultant shifts towards higher binding energy, as illustrated in Fig. 3(b). An increase in C 1s peak intensity with significant contributions from CO and COO signals at 286.2 and 288.5 eV, respectively, indicated the citrate coating on AuNPs as shown in Fig. 3(c). The Au $4f_{7/2}$ peak appeared at 83.8 eV [Fig. 4(c)], demonstrating the immobilization of AuNPs onto the ITO surface. A summary of the normalized elemental compositions of all samples is shown in Table 1 to substantiate the progress in each step of fabrication. The O 1s signal intensity increased significantly due to the photodegradation of ODS molecules and the formation of siloxane/silanol moieties, which attract the APS molecules.

The surface modification presented here involves the photodegradation of the ODS monolayer at selected sites, followed by the backfilling of the VUV-exposed area by APS molecules. This strategy provides a chemically manipulated template for immobilizing the AuNPs at predefined sites. By use of different surfactants with various chemical functional groups and/or nanoparticle composition and size, promises potential applications in electronic and optical devices fabrication, patterning of biologically active species, and catalysis at selected areas, for example.

4. Conclusions

We successfully immobilized AuNPs into two-dimensional arrays on predefined sites on ITO. A chemical template with alternating linear features of ODS and APS monolayers was fabricated by photolithography. This microstructured surface was used for controlled site-selective immobilization of AuNPs. Electrostatic interaction between citrate-capped AuNPs and the amino-terminated monolayer was

the driving force behind this fabrication, which allows AuNPs to be placed at amino-terminated sites while the methyl-terminated monolayer (masked linear features) remains unexposed to AuNPs. By selecting an appropriate colloidal solution and surfactant, our microfabrication strategy demonstrated herein can be applied for the preparation of different types of microstructured features on the surface.

Acknowledgement

The authors are grateful to Professor M. Oyama, International Innovation Center (IIC), Kyoto University, and Professor Y. Awakura for allowing the use of the FE-SEM and SEM facilities, respectively, for performing this work. They also acknowledge the help of Mr. K. Adachi and Mr. A. Ito for their support in utilizing the FE-SEM and SEM facilities. This work was supported by Grants-in-Aid for Scientific Research on Priority Area "Strong photons-molecules coupling fields (No. 470)" and on Scientific Research Category A (No. 17206073) from the Ministry of Education, Culture, Sports, Science and Technology of Japan. Author O. P. Khatri gratefully acknowledges the Japan Society for the Promotion of Science (JSPS) for the JSPS postdoctoral fellowship.

References

1) M. C. Daniel and D. Astruc: Chem. Rev. **104** (2004) 293.
2) A. N. Shipway, E. Katz, and I. Willner: ChemPhysChem **1** (2000) 18.
3) S. A. Choulis, M. K. Mathai, and V. Choong: Appl. Phys. Lett. **88** (2006) 213503.
4) S. A. Maier and H. A. Atwater: J. Appl. Phys. **98** (2005) 011101.
5) Y. Sun and Y. Xia: Science **298** (2002) 2176.
6) K. L. Kelly, E. Coronado, L. L. Zhao, and G. C. Schatz: J. Phys. Chem. B **107** (2003) 668.
7) W. Rechberger, A. Hohenau, A. Leitner, J.R. Krenn, B. Lamprecht and F.R. Aussenegg: Opt. Commun. **220** (2003) 137.
8) H. X. He, H. Zhang, Q. G. Li, T. Zhu, S. F. Y. Li, and Z. F. Liu: Langmuir **16** (2000) 3846.
9) X. Ling, X. Zhu, J. Zhang, T. Zhu, M. Liu, L. Tong, and Z. Liu: J. Phys. Chem. B **109** (2005) 2657.
10) W. Cheng, S. Dong, and E. Wang: J. Phys. Chem. B **108** (2004) 19146
11) X. Zhang, E. M. Hicks, J. Zhao, G. C. Schatz, and R. P. Van Duyne: Nano Lett. **5** (2005) 1503.
12) S. Linden, J. Kuhl, and H. Giessen: Phys. Rev. Lett. **86** (2001) 4688.
13) V. Santhanam and R. P. Andres: Nano Lett. **4** (2004) 41.
14) B. D. Gates, Q. Xu, M. Stewart, D. Ryan, C. G. Willson, and G. M. Whitesides: Chem. Rev. **105** (2005) 1171
15) Y. Xia and G. M. Whitesides: Angew. Chem. Int. Ed. **37** (1998) 550
16) D. S. Ginger, H. Zhang, and C. A. Mirkin: Angew. Chem. Int. Ed. **43** (2004) 30.
17) K. Lee, F. Pen, G. T. Carroll, N. J. Turro, and J. T. Koberstein: Langmuir **20** (2004) 1812.
18) H. Sugimura, K. Ushiyama, A. Hozumi, and O. Takai: Langmuir **16** (2000) 885.

19) R. B. A. Sharpe, D. Burdinski, C. V. Marel, J. A. J. Jansen, J. Huskens, H. J. W. Zandvliet, D. N. Reinhoudt, and B. Poelsema: Langmuir **22** (2006) 5945.

20) F-E. Truica-Marasescu and M. R. Wertheimer: Macromol. Chem. Phys. **206** (2005) 744.

21) H. Sugimura, K-H. Lee, H. Sano, and R. Toyokawa: Colloid Surf. A **284-285** (2006) 561

22) H. Sugimura and N. Nakagiri: Appl. Phys. A **66** (1998) S427.

23) Y. Fukushi, H. Kominami, Y. Nakanishi, and Y. Hatanaka: Appl. Surf. Sci. **244** (2005) 537.

24) H. Sugimura, A. Hozumi, T. Kameyama, and O. Takai: Surf. Interface Anal. **34** (2002) 550.

25) A. C. Fozza, J. Roch, J. E. K lemberg-Sapieha, A. Kruse, A. Hollander, and M. R. Wertheimer: Nucl. Instrum. Methods Phys. Res. B **131** (1997) 205

26) A. N. Shipway, M. Lahav, and I. Willner: Adv. Mater. **12** (2000) 993.

27) O. P. Khatri, K. Murase, and H. Sugimura: in preparation for publication.

28) D. Briggs: in *Surface Analysis of Polymers by XPS and Static SIMS* (Cambridge University Press, New York, 1998) p. 65.

Figure Captions

Fig. 1: Schematic view of immobilization of AuNPs in linear fashion onto the ITO surface. This multistep process includes the (a) self-assembly of ODS monolayer and VUV irradiation for 10 min, (b) formation of silanol and/or siloxane moieties on VUV exposed sites, (c) self-assembly of APS monolayer on VUV patterned sites, and (d) immobilization of AuNPs on predefined APS sites.

Fig. 2: (a) SEM image of ITO with predefined immobilization of AuNPs arrays in linear fashion. Bright and dark linear features represent AuNPs arrays and ODS monolayer respectively. (b) FESEM image of scattered organization of AuNPs on APS-modified sites at higher magnification. This image shows part of the bright feature, shown in (a).

Fig. 3: XPS spectra of C 1s after (a) VUV patterning on the ODS monolayer, (b) back-filling of APS monolayer on VUV-exposed sites, and (c) immobilization of AuNPs on predefined sites.

Fig. 4: XPS spectra of (a) Si 2p, (b) C 1s, and (c) Au 4f. Intensities of these elements indicate the different steps of the immobilization of AuNPs on predefined sites. Each figure contains four curves that represent the (A) self-assembly of ODS monolayer, (B) VUV patterning on ODS monolayer, (C) backfilling of APS monolayer on VUV-exposed sites, and (D) immobilization of AuNPs on predefined sites.

Table 1: Chemical quantification of ITO surfaces at each step of fabrication, as determined by XPS.

Fabrication step*	Elemental composition (%)						
	O 1s	Sn 3d	In 3d	N 1s	C 1s	Si 2p	Au 4f
A	41.3	1.7	25.4	0	28.1	3.5	0
B	51.0	2.0	30.0	0	13.6	3.4	0
C	46.1	1.9	26.3	0.7	20.1	4.9	0
D	43.2	1.8	24.1	0.6	24.0	4.6	1.7

*A: ODS monolayer deposited on ITO, B: followed by VUV lithography, C: backfilling by APS molecules on VUV exposed sites, and D: Immobilization of AuNPs onto the predefined sites.

Fig. 1

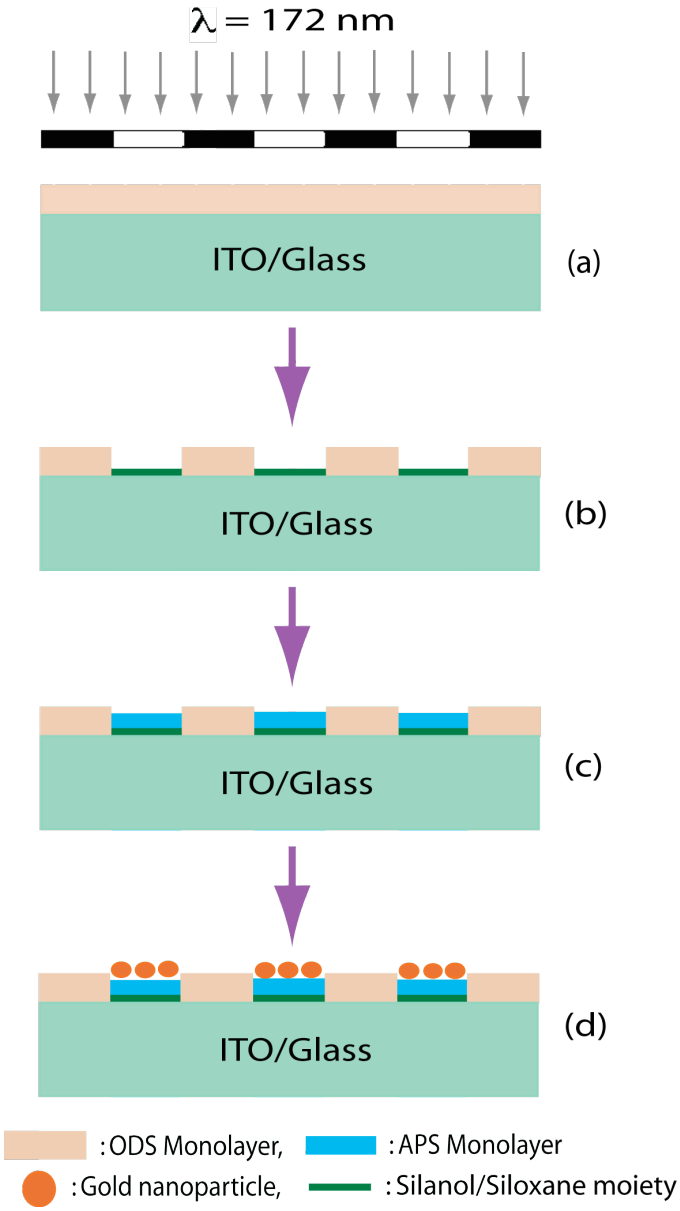
λ = 172 nm
ITO/Glass
(a)
ITO/Glass
(b)
ITO/Glass
(c)
ITO/Glass
(d)
: ODS Monolayer,
: APS Monolayer
: Gold nanoparticle,
: Silanol/Siloxane moiety

Fig. 2

(a)

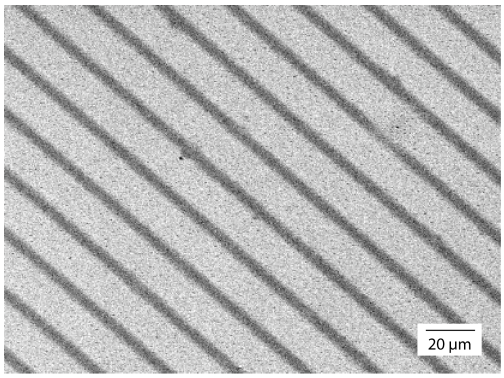

(b)

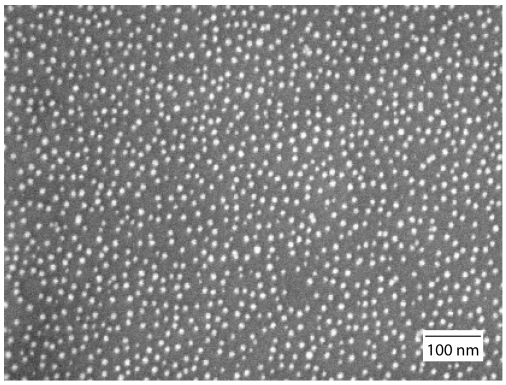

Fig. 3

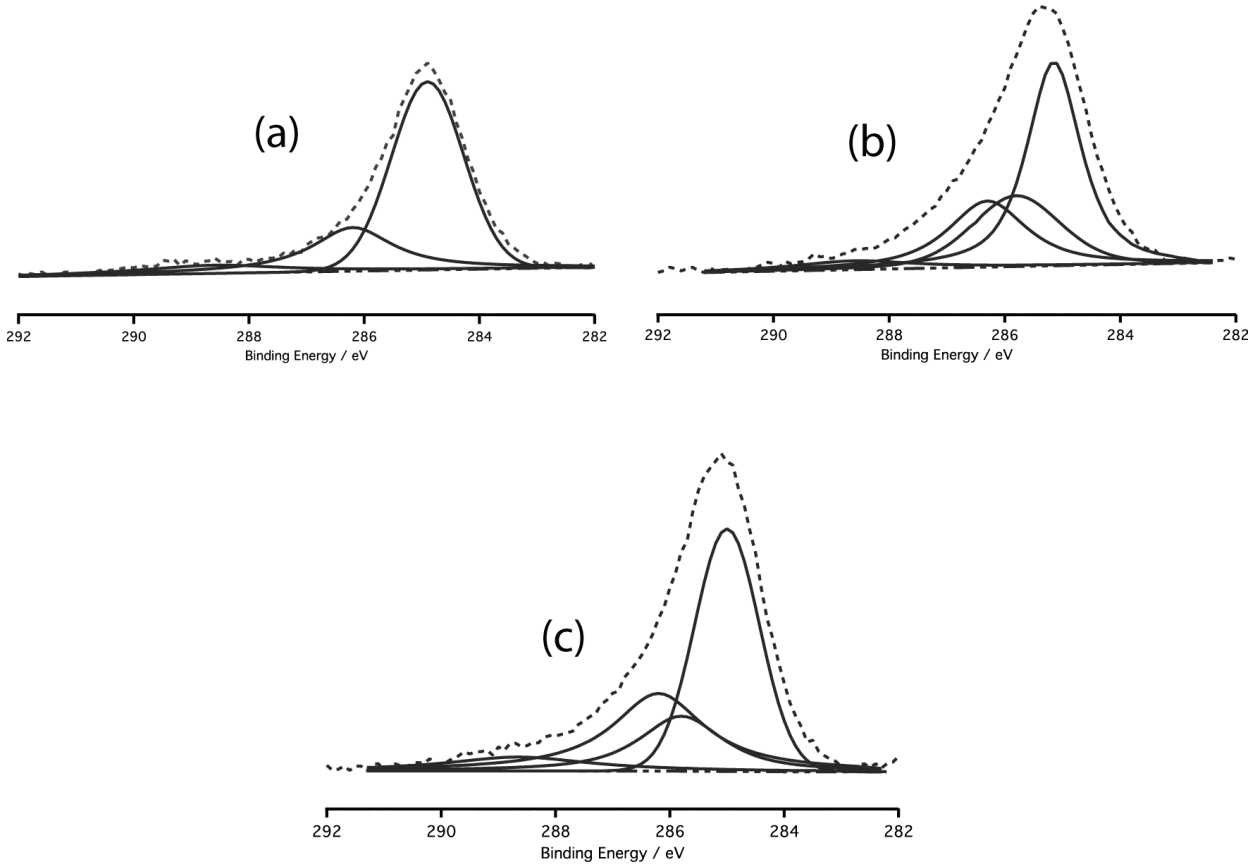
(a)
292
290
288
286
284
282
Binding Energy / eV
(b)
292
290
288
286
284
282
Binding Energy / eV
(c)
292
290
288
286
284
282
Binding Energy / eV

Fig. 4

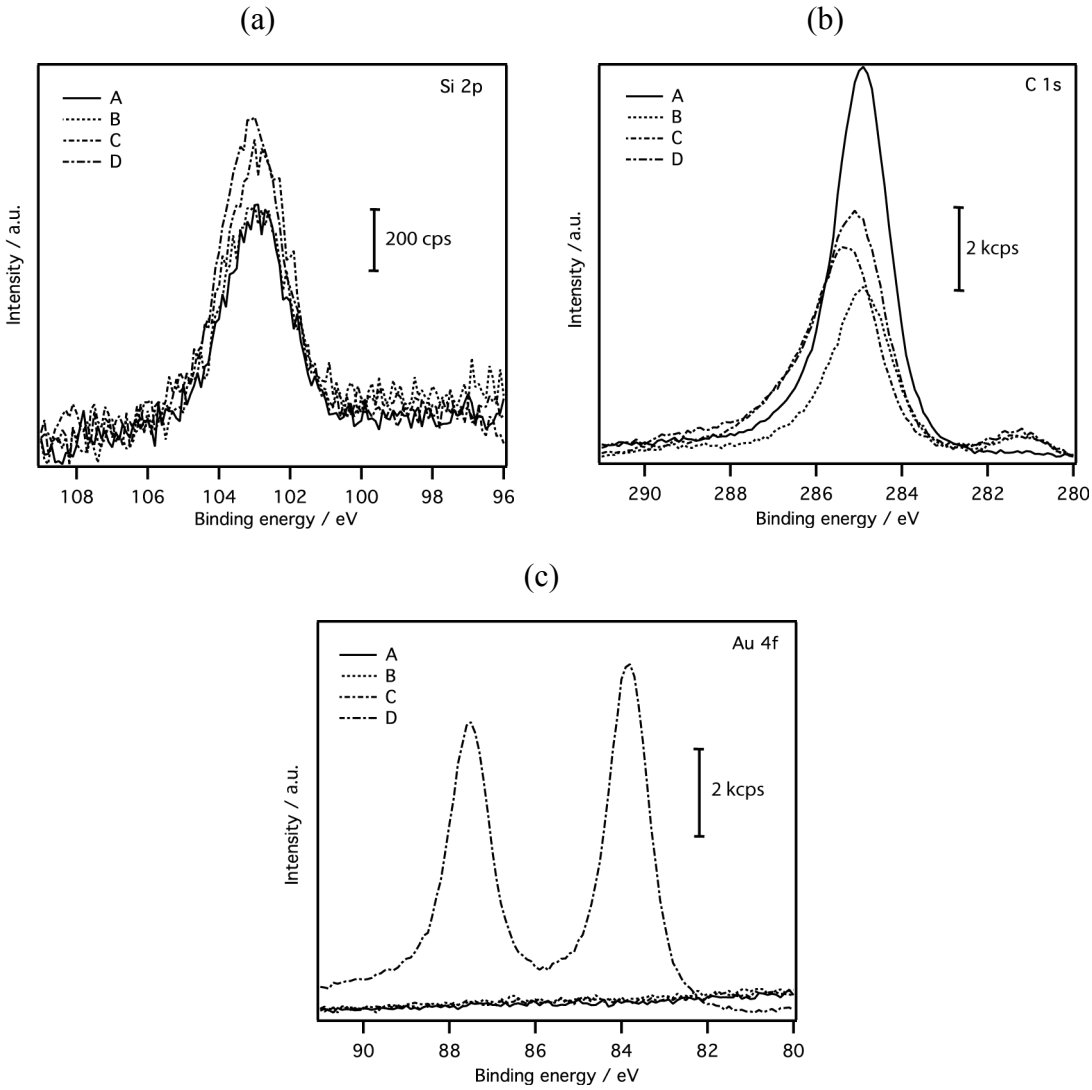
(a)
(b)
(c)
A
B
C
D
Si 2p
200 cps
Intensity / a.u.
108
106
104
102
100
98
96
Binding energy / eV
C 1s
2 kcps
290
288
286
284
282
280
Au 4f
90
88
86
84
82
80